

**EPITAXIAL GROWTH OF III-V NITRIDES
BASED LIGHT EMITTING DIODES BY METAL
ORGANIC CHEMICAL VAPOR DEPOSITION**

MUHAMMAD ESMED ALIF BIN SAMSUDIN

UNIVERSITI SAINS MALAYSIA

2023

**EPITAXIAL GROWTH OF III-V NITRIDES
BASED LIGHT EMITTING DIODES BY METAL
ORGANIC CHEMICAL VAPOR DEPOSITION**

by

MUHAMMAD ESMED ALIF BIN SAMSUDIN

**Thesis submitted in fulfilment of the requirements
for the degree of
Doctor of Philosophy**

March 2023

ACKNOWLEDGEMENT

Alhamdulillah, syukran, by the grace of The Almighty, I was able to complete this thesis. Let every single things that happened during the completion of the thesis be the greatest experience to my life. First and foremost, I would like to thank my supervisor, Associate Professor Dr. Norzaini Zainal, for her invaluable guidance, encouragement, and constructive comments throughout my research. She consistently checked my papers and thesis, despite her busy schedule. Her zeal in nitride epitaxy inspires me to learn more about it. I would also like to thank my co-supervisor, Professor Steven DenBaars, for his invaluable advice and assistance towards my project. Also, many thanks to Professor James Speck, Professor Shuji Nakamura and Mike for their support and fantastic discussions during my 9-month training at UCSB.

This research would not be completed without financial support from various research grants from Ministry of Education. Many thanks to Collaborative Research in Engineering, Science and Technology (CREST) for initiating Nitride epitaxy in Malaysia and their continuous support in this research, especially for MOCVD maintenance at INOR. To my 'long-served' colleagues, Ikram, Ezzah, Waheeda and Yusnizam, thank you for your contributions and being helpful during my hard and ease time. Technical assistance from INOR and School of Physics staffs is greatly appreciated.

On this occasion, I dedicated this thesis to my mother for her blessing and dua'a. Not to be forgotten, Al-Fatihah (read) to my late father. To my lovely siblings, thank you for your encouragement and support. To my parent-in-laws, thank you for your patience, prayers and supports. Last but not least, I would like to express my heartfelt gratitude to my soulmate, Syara, who have been stood by me through thick and thin, during the completion of this thesis. To my son, Aisy, I love you 3000.

TABLE OF CONTENTS

ACKNOWLEDGEMENT	ii
TABLE OF CONTENTS	iii
LIST OF TABLES	vi
LIST OF FIGURES	viii
LIST OF SYMBOLS	xiv
LIST OF ABBREVIATIONS	xv
LIST OF APPENDICES	xvii
ABSTRAK	xviii
ABSTRACT	xx
CHAPTER 1 INTRODUCTION TO III-V NITRIDE SEMICONDUCTOR	1
1.1 Challenges in developing blue and UV LEDs	2
1.2 Problem statement and novelty of the research.....	4
1.3 Aim and objectives of research	7
1.4 Scope of research	7
1.5 Outline of the thesis	9
CHAPTER 2 LITERATURE REVIEW	12
2.1 Introduction to III-V Nitride materials.....	12
2.2 Basic concept of LED and its terminology	16
2.2.1 Radiative and non-radiative recombination.....	17
2.2.2 Quantum confinement stark effect in nitride LEDs	18
2.2.3 Definitions of LED efficiencies	19
2.2.4 Carrier screening and band-filling effect in InGaN based LEDs.....	21
2.2.3 Carrier localization in InGaN based LEDs.	23
2.3 Issues and challenges in InGaN based LED development for visible lighting ...	25
2.3.1 Basic InGaN based LED epilayer structure and its typical issue.....	25
2.3.2 Reducing threading dislocations in GaN layer on sapphire.....	28
2.3.2(a) Review of GaN nucleation on patterned sapphire substrate (PSS).....	35
2.3.3 Improvement of LED performance by superlattices (SLs).....	37
2.3.4 Comparison of InGaN/GaN LED grown on sapphire and on bulk GaN	39

2.4	Issues and challenges in AlGaIn based LED development for UV lighting	41
2.4.1	Basic AlGaIn based LED epilayer structure and its typical issue	41
2.4.2	Reducing threading dislocation in AlN layer on sapphire	44
2.4.3	Potential of growing AlN layer at low temperature	50
2.5	Summary	55
CHAPTER 3 RESEARCH METHODOLOGY		56
3.1	Development of InGaIn based LEDs	56
3.1.1	Preparation of GaN growth on PSS as a base layer for InGaIn based LED	58
3.1.2	Growth of GaN nucleation for GaN overgrown layer	59
3.1.3	Growth of InGaIn based LEDs on PSS	60
3.1.4	Introduction of superlattices (SLs) in InGaIn based LEDs	62
3.1.5	Growth of InGaIn based LEDs on GaN substrate	64
3.1.6	Fabrication of InGaIn based LEDs	67
3.1.7	Packaging of InGaIn based LEDs	72
3.2	Development of AlGaIn based LEDs	75
3.2.1	Preparation of AlN growth on sapphire substrate as a base layer for AlGaIn based LEDs	76
3.2.2	Nitridation and growth of AlN nucleation for AlN overgrown layer	78
3.2.3	Growth of low temperature grown AlN layer at 1175 °C by controlling TMAI preflow times	80
3.2.4	Growth of AlGaIn based LEDs on selected AlN overgrown layer	82
3.3	Characterizations of LEDs	84
3.3.1	Surface measurement	84
3.3.2	Crystalline and composition measurement	87
3.3.3	Optical measurement	94
3.3.4	Optical-electrical measurement for LEDs	96
3.4	Summary	99
CHAPTER 4 RESULTS AND DISCUSSIONS		100
4.1	Epitaxial growth of InGaIn based LEDs for visible lighting	100
4.1.1	Reduction of threading dislocations in GaN on PSS by controlling growth temperature of GaN nucleation	101

4.1.2	Improvement of LED performance by controlling number of period and indium composition of InGaN/GaN superlattices.	108
4.1.3	Comparison of InGaN/GaN LED grown on PSS and on bulk GaN.....	117
4.2	Epitaxial growth of AlGaN based LED for UV lighting	134
4.2.1	Growth of AlN layer on sapphire substrate as a base layer for AlGaN based LEDs by controlling nitridation time.....	135
4.2.2	Growth of AlN layer on sapphire substrate as a base layer for AlGaN based LEDs by controlling nucleation thickness of AlN layer.....	142
4.2.3	Growth of AlN layer at a low temperature of 1175 °C by controlling TMAI preflow times	150
4.2.4	Growth of AlGaN based LEDs on AlN layers.....	155
4.3	Summary	157
CHAPTER 5 CONCLUSION AND FUTURE WORKS.....		159
5.1	Conclusion	159
5.2	Recommendations for Future Research	161
REFERENCES.....		164
APPENDICES		
LIST OF PUBLICATIONS		

LIST OF TABLES

		Page
Table 2.1	Common parameters of binary III-nitride materials at 300 K. The values were taken from [28-29,24-26].	15
Table 2.2	Summary of epilayer design which can influence the performance of InGaN based LEDs.	28
Table 2.3	Comparison of lattice mismatch of GaN with respect to different substrates [78].	31
Table 2.4	Reported methods in reducing threading dislocation (TDs) for GaN layer.	34
Table 2.5	Summary of key parameters for GaN nucleation control.	37
Table 2.6	Summary of epilayer design which can influence the performance of AlGaN based LEDs.	44
Table 2.7	Comparison of lattice mismatch of AlN with respect to different substrates [78].	45
Table 2.8	Reported methods in reducing threading dislocation (TDs) for AlN layer.	49
Table 2.9	Review on the growth of AlN layer at temperature below 1200 °C	54
Table 3.1	Details of GaN layers grown with different nucleation temperatures.	60
Table 3.2	Summary of studied parameters for InGaN based LEDs grown with different SLs periods using 5% and 4% of indium composition, respectively.	62
Table 4.1	Details of XRD results along with estimation of TDs for GaN layers grown with different nucleation temperatures.	103
Table 4.2	Comparison of benchmarking GaN nucleation temperature layer on PSS across recent findings.	106
Table 4.3	Summary of estimated V-pits size for InGaN based LEDs grown with different SLs periods using different In compositions	114
Table 4.4	Details of XRD results along with estimation of TDs for LED I and LED II	121
Table 4.5	Details of fitted activation energies for LED I and LED II.	132

Table 4.6	Summary of PL peak intensity and its estimated IQE for LED I and LED II.....	134
Table 4.7	Estimated density for screw dislocations, edge dislocations, and threading dislocations of AlN layer with different nitridation time.	142
Table 4.8	Estimated density for screw dislocation, edge dislocation, and threading dislocations of AlN layer with different nucleation thicknesses.....	147
Table 4.9	Estimated density of screw dislocation, edge dislocation, and threading dislocations density of low temperature AlN layer with different TMAI preflow times.	154

LIST OF FIGURES

	Page
Figure 2.1	Energy band diagram of III-V nitrides in the function of lattice constant a at room temperature. Image taken from [26] 13
Figure 2.2	Atomic arrangement for wurtzite structure of nitride materials. The images were taken from [27]..... 14
Figure 2.3	Basic working principal of an LED [26]. 17
Figure 2.4	Formation of QCSE in nitride LED. Image taken and edited from [47]..... 19
Figure 2.5	The schematic diagram for (a) screening effect and (b) band filling effect in the InGaN based LEDs. Image taken and edited from [57]..... 22
Figure 2.6	Illustration of thermal quenching in QW. Image taken and edited from [61]..... 24
Figure 2.7	General design of InGaN based LED structure. 25
Figure 2.8	Mechanism of TDs propagation in common InGaN based LED structure. 29
Figure 2.9	IQE as a function of dislocation density at different current densities for a reported InGaN based LEDs. Image taken and edited from [76]..... 30
Figure 2.10	Light extraction of LED grown on PSS and planar substrate. Image was taken and edited from [84]. 33
Figure 2.11	Mechanism of dislocation inclination in GaN layer, image taken and edited from [90].. 36
Figure 2.12	Reported cross-sectional TEM image showing a representative of typical V-pits structure in an InGaN based LED by [25]..... 38
Figure 2.13	General design of AlGaN based LED structure 42
Figure 2.14	Correlation of IQE of AlGaN based LED as a function of dislocation density [106]. 45
Figure 2.15	Illustration of schematic mechanism of AlN layer, with and without AlON formation, proposed by [114]. 51

Figure 3.1	Flow chart of InGaN based LEDs on patterned sapphire substrate for developing an LED with improved performance.	57
Figure 3.2	Growth temperature profile of the GaN layer grown with nucleation on PSS.....	60
Figure 3.3	Schematic diagram of InGaN based LED grown on the GaN layer with the optimized nucleation temperature.	61
Figure 3.4	InGaN based LED structure grown on PSS using atmospheric pressure MOCVD reactor, as demonstrated in this work.....	63
Figure 3.5	Growth temperature profile of the InGaN based LED grown on PSS	63
Figure 3.6	Schematic diagram of sapphire corral for LED on bulk GaN growth.....	64
Figure 3.7	InGaN based LED structure grown on bulk GaN substrate using atmospheric pressure MOCVD reactor, as demonstrated in this work.....	66
Figure 3.8	Growth temperature profile of the InGaN based LED grown on GaN.....	66
Figure 3.9	(a) ITO deposition, (b) mesa patterns after UV exposure and (c) mesa patterns as seen under optical microscope.	68
Figure 3.10	Steps of forming mesas on an LED wafer, as demonstrated in this work.....	69
Figure 3.11	(a) Formation of n-contact on an InGaN based LED, (b) top-view of n-metal contact structure as observed under optical microscope.....	71
Figure 3.12	(a) Formation of p-contacts and n-contacts on an InGaN based LEDs, (b) top-view of fabricated LEDs structures as observed under optical microscope.....	72
Figure 3.13	(a) Illustration of two-steps dicing and (b) microscope image of the successful LEDs singulation.....	73
Figure 3.14	(a) Mounted LED on silver header and (b) microscope image of the successful wire-bonded LED device.	74
Figure 3.15	Flow chart of AlGaN based UV-C LEDs on sapphire substrate.	76
Figure 3.16	Schematic diagram of horizontal flow MOCVD reactor with division of stream parts and inlets used for AlGaN based LED	

	growth. The image was taken from technical report, which provided by TNSC [121].	77
Figure 3.17	Growth temperature profile of AlN layer on sapphire at high temperature	79
Figure 3.18	Growth temperature profile of AlN layer on sapphire at 1175°C	81
Figure 3.19	Growth temperature profile of the AlGaN based LED grown on sapphire	83
Figure 3.20	Schematic diagram of AlGaN based LED structure grown on the selected AlN layers	84
Figure 3.21	An example of basic diagram of SEM system. Image was taken and edited from [124]	85
Figure 3.22	An example of AFM system taken from [125]	87
Figure 3.23	Mechanical arms and gonio system with key components for a standard XRD system	88
Figure 3.24	Example of XRD results of (002) and (102) scans for GaN layer	90
Figure 3.25	Example of XRD ω -2 θ scan for single layer a) InGaN and b) AlGaN layer	91
Figure 3.26	The illustration of X-ray photoelectron spectroscopy measurement. Image was modified from [133]	93
Figure 3.27	A reported XPS spectra of N 1s core level for AlN surface [134]	94
Figure 3.28	Schematic diagram of temperature dependent PL measurement in this work	96
Figure 3.29	Schematic diagram for the QT setup for both USM and UCSB	97
Figure 3.30	Schematic diagram of integrated sphere setup used in this work	98
Figure 3.31	Schematic diagram of 4π configuration setting in this work. Image is taken and modified from manual book ISP 500 [88]	98
Figure 4.1	XRD ω -scans in (a) (002) and (b) (102) reflection for GaN on different nucleation temperatures. Inset: FWHMs of XRD ω -scans with respect to temperature	102
Figure 4.2	Estimated TDs density for GaN layers grown with different nucleation temperatures	103
Figure 4.3	Surface roughness of GaN layers grown with different growth temperature	104

Figure 4.4	AFM 2D images of GaN layers grown with different growth temperature.	105
Figure 4.5	(a) light output power and (b) I-V characterization on LEDs. This measurement was measured on LED wafers.	107
Figure 4.6	(a) Light output power and (b) I-V characteristic of InGaN based LEDs grown without and with SLs at different periods for In _{0.05} Ga _{0.95} N based SLs.	109
Figure 4.7	AFM 2D images of InGaN based LEDs grown without and with SLs at different period for 5 % of In in SLs.	110
Figure 4.8	(a) Light output power and (b) I-V characteristic of InGaN based LED grown without and with SLs at different periods for In _{0.04} Ga _{0.96} N based SLs.	112
Figure 4.9	AFM 2D images of InGaN based LEDs grown without and with SLs at different period for 4 % of In in SLs.	113
Figure 4.10	(a) AFM 2D image (b) depth profile of V-pits on the LED with InGaN SLs at 4% and 20 periods. White box on (a) shows the measured area for the depth profile.	115
Figure 4.11	A reported V-pit structure on InGaN based LED as observed through TEM measurement. Inset figure shows the AFM image of the InGaN based LEDs surface. Image was taken and edited from [7].	116
Figure 4.12	SEM cross-sectional images of the (a) PSS and (b) roughened N-face of the GaN substrate.	119
Figure 4.13	XRD ω -scans in (a) (002) and (b) (102) reflections for both LEDs	120
Figure 4.14	XRD ω -2 θ scans in (004) reflection for LED I and LED II.	122
Figure 4.15	FWHM as a function of peak/fringe order with fitted line.	123
Figure 4.16	EL spectra for LED I and LED II at a current of 20 A/cm ²	124
Figure 4.17	(a-b) EL spectra and (c) fluctuation of the EL peak wavelength as a function of current density for LED I and LED II.	125
Figure 4.18	Voltage as functions of current for LED I and LED II.	126
Figure 4.19	AFM surface for (a) LED I and (b) LED II. (c) AFM depth profile for surface of LED I, where V-pits present from scanned area (yellow circle).	127

Figure 4.20	Light output power as a function of current density for LED I and LED II.....	128
Figure 4.21.	EQE as a function of current for LED I and LED II.	129
Figure 4.22	PL spectra for (a) LED I and (a) LED II measured temperature from 10 to 300 K.	131
Figure 4.23	Arrhenius graph of temperature dependent PL for (a) LED I and (b) LED II.....	132
Figure 4.24	PL peak intensity for (a) LED I and (b) LED II, measured at 300 K and 10 K.....	133
Figure 4.25	RMS surface roughness for the surface of the AlN layers grown with different nitridation times. The solid line is only a guideline to eye.	136
Figure 4.26	AFM 2D images of AlN layer grown on (a) without nitridation, (b) with 20 minutes, and (c) with 60 minutes.....	137
Figure 4.27	Depth profile for AlN layer grown (a) without nitridation, (b) with 20 minutes, and (c) with 60 minutes of nitridation. The results were taken from AFM measurement.	138
Figure 4.28	High resolution XPS spectra of N 1s for (a) 20 minutes and (b) 60 minutes of nitridation.	140
Figure 4.29	XRD ω -scans in (a) (002) and (b) (102) reflection for AlN on different nitridation times. Inset: FWHMs of XRD ω -scans with respect to time.....	141
Figure 4.30	RMS roughness for the surface of AlN layer grown with different nucleation thicknesses.	143
Figure 4.31	AFM 2D images of AlN layer grown on (a) without nucleation, (b) with 5 nm, (c) with 10 nm and (d) with 20 nm.....	144
Figure 4.32	Depth profile for AlN layers grown (a) without nucleation, (b) with 5 nm (c) 10 nm, and (d) with 20 nm of nucleation. The results were taken from AFM measurement.....	145
Figure 4.33	XRD ω -scans in (a) (002) and (b) (102) reflection for AlN on different nucleation thicknesses. Inset: FWHMs of XRD ω -scans with respect to thickness	146

Figure 4.34	(a) RMS surface roughness of AlN nucleation with different thickness. AFM 2D-images of $1\mu\text{m} \times 1\mu\text{m}$ for the surface of the corresponding nucleation thickness.....	148
Figure 4.35	RMS surface roughness of AlN layers grown with different TMAI preflow times.	151
Figure 4.36	AFM 2D images of AlN layer grown on (a) without TMAI preflow (b) 10 seconds, (c) 20 seconds, (d) 30 seconds, (e) 45 seconds and (f) 60 seconds.	152
Figure 4.37	XRD ω -scans in (a) (002) and (b) (102) reflection for AlN on different TMAI preflows. Inset: FWHMs of XRD ω -scans with respect to preflow times.	153
Figure 4.38	Cathodoluminescence (CL) spectra for (a) LED A, and (b) LED B	156
Figure 4.39	(a) I-V characteristic measured on UV-C LED wafers.	157

LIST OF SYMBOLS

$^{\circ}$	Degree
$^{\circ}\text{C}$	Temperature in degree celcius
2θ	Diffraction angle in XRD (2 Theta)
a	Lattice constant in a -plane
\AA	Angstrom
b_a	Burger vector in a -plane
c	Lattice constant in c -plane
K	Temperature in Kelvin
ϕ	in-plane rocking curve
β	Integral width (FWHM)
λ	wavelength
ω	Diffraction angle in XRD (Omega)

LIST OF ABBREVIATION

2D	Two-dimensional
3D	Three-dimensional
Al	Aluminium
Al ₂ O ₃	Sapphire
AlGaN	Aluminum gallium nitride
AlN	Aluminium Nitride
AlON	Aluminum oxynitride
atm	Standard atmospheric pressure
ATP	Atom probe topography
Au	Gold
CL	Cathodoluminescence
Cp ₂ Mg	Bis(cyclopentadienyl)magnesium
Cr	Chromium
DI	Deionized
E-beam	Electron beam
EBL	electron blocking layer
EDs	edge dislocations density
EL	Electroluminescence
ELOG	epitaxial lateral overgrowth
EQE	External quantum efficiency
ETD	Everhart-Thornley Detector
FEG	Field emission Gun
FESEM	Field Emission Scanning Electron Microscopy
FWHM	Full Width of Half Maximum
Ga	Gallium atom
Ga	Gallium
GaN	Gallium Nitride
H ₂	Hydrogen
H ₂ O	Water
H ₂ O ₂	Hydrogen Peroxide
HCL	Hydrochloric Acid
HMDS	hexamethyldisilazane
HVPE	Hydride vapor phase epitaxy
ICP	inductively coupled plasma
In	Indium
InGaN	Indium gallium nitride
InN	Indium nitride
IQE	Internal quantum efficiency
IR	Infra red
ITO	Indium Tin oxide
LEDs	Light Emitting Diodes
LOP	Light output power
MBE	Molecular Beam Epitaxy

MFC	Mass Flow Controller
Mg	magnesium
MHA	methane-Hydrogen-Argon
ML	Multilayer
MO	Metal organic
MOCVD	Metal Organic Chemical Vapor Deposition
MQW	Multiquantum well
N	Nitrogen atom
N ₂	Nitrogen gas
NH ₃	Ammonia
Ni	Nickel
NMP	1-methyl-2-pyrrolidone
PALE	pulse atomic layer epitaxy
PL	Photoluminescence
PR	Photoresist
PSS	patterned sapphire substrate
QCSE	quantum confinement stark effect
QT	quick-test
RC	Rocking curve (XRD)
RCA	Radio Corporation of America
RF	Radio frequency
RMS	Root Mean Square
SCCM	Standard Cubic Centimeters per Minute
SDs	screw dislocations density
SDGs	Sustainable development goals
Si	Silicon
Si ₂ H ₆	Disilane
SiC	Silicon Carbide
SLM	Standard Litres per Minute
SLs	Superlattices
SSL	Solid State Lighting
TDs	Threading dislocations density
TEGa	Triethylgallium
TEM	Transmission electron microscopy
Ti	Titanium
TMAI	Trimethylaluminum
TMGa	Trimethylgallium
TNSC	Taiyo Nippon Sanso
UID	unintentionally doped
UV	Ultraviolet
XRD	X-ray Diffraction
XPS	X-ray Photoelectron spectroscopy
YL	Yellow luminescence

LIST OF APPENDICES

- Appendix A Example of calculation of the estimated threading dislocation density
- Appendix B Calibration of growth rate for low temperature GaN
- Appendix C Summary of fabrication process to form functional LED on wafer
- Appendix D Summary of packaging process to form Functional LED Device
- Appendix E Graph of dependence of AlN growth rate with respect to temperature, pressure, ammonia flow and TMAI flow
- Appendix F Example of ‘best fit’ simulation to measure the thickness of multi-quantum well and barrier for an InGaN based LEDs by x’pert epitaxy software.
- Appendix G: Evidence of 20 periods of SLs and 6 MQWs for the sister wafer of InGaN based LEDs grown at USM with similar LED structure grown at UCSB.

**PENUMBUHAN EPITAKSI DIOD PEMANCAR CAHAYA BERASASKAN
III-V NITRIDA MENGGUNAKAN PEMENDAPAN WAP KIMIA LOGAM
ORGANIK**

ABSTRAK

Kajian ini bertujuan untuk meningkatkan prestasi LED berasaskan indium gallium nitrida (InGaN) dan menghasilkan LED berasaskan aluminum gallium nitrida (AlGaN) yang berfungsi melalui epitaksi pemendapan wap kimia logam organik. Kesan suhu pertumbuhan lapisan nukleasi gallium nitrida (GaN), bilangan lapisan kekisi berulang dan komposisi indium didalamnya terhadap prestasi LED berasaskan InGaN telah dikaji. Didapati penumbuhan nukleasi GaN pada suhu 570 °C mampu menurunkan perkehelan berulir didalam lapisan GaN yang ditumbuhkan (yang menjadi lapisan asas kepada LED). Pada suhu nukleasi 570 °C, pertumbuhan 3D (pulau-pulau) yang lebih besar terbentuk dan menggalakkan kecenderungan pemansuhan kehelan, dan mengurangkan perkehelan berulir. Seterusnya, penumbuhan 20 bilangan lapisan kekisi berulang $\text{In}_{0.04}\text{Ga}_{0.96}\text{N}/\text{GaN}$ menghasilkan saiz liang-V yang bersesuaian. Ini dapat meningkatkan suntikan lubang kedalam telaga - quantum dan seterusnya meningkatkan prestasi LED. Kajian ini juga melakukan percubaan untuk mengetahui faktor yang menghadkan penggunaan substrat GaN dalam pembangunan LED berasaskan InGaN berbanding substrat saphir, terutamanya substrat saphir bercorak (PSS), yang digunakan secara meluas dalam kebanyakan kajian, termasuk dalam kajian ini. Keputusan menunjukkan LED pada PSS berprestasi lebih baik daripada LED pada GaN, walaupun LED pada GaN mempunyai perkehelan berulir yang lebih rendah. Pembentukan liang-V dan lokalisasi pembawa, yang lebih

ketara didalam LED pada PSS berbanding LED pada GaN, mendorong kepada penghasilan voltan hadapan yang rendah dan penggabungan sinaran yang lebih tinggi dan seterusnya meningkatkan prestasi LED. Untuk kajian seterusnya, pengaruh masa nitridasi, ketebalan nukleasi AlN dan masa pra-aliran aluminium,trimetil- (TMAI) untuk LED berasaskan AlGaIn telah dijalankan. Perkehelan berulir didalam lapisan AlN yang ditumbuhkan pada suhu 1340 °C (yang menjadi lapisan asas kepada LED) berkurangan apabila 20 minit masa nitridasi digunakan. Aluminium oxinitrida yang terhasil daripada nitridasi, dapat mengurangkan perkehelan berulir. Seterusnya perkehelan berulir dapat dikurangkan lagi dengan menggunakan 10 nm lapisan nukleasi AlN. Dalam keadaan ini, pertumbuhan 3D bersesuaian untuk menggalakkan kecenderungan pemansuhan kehelan pada lapisan AlN yang ditumbuhkan. Kajian ini juga melakukan percubaan untuk menumbuhkan lapisan AlN pada suhu 1175 °C. Untuk meningkatkan kualiti AlN, masa pra-aliran TMAI telah dioptimumkan selepas lapisan nukleasi. Dengan pra-aliran TMAI selama 30 saat, ketakutan campuran Al dan N dapat dikurangkan serta melicinkan permukaan AlN. Seterusnya, LED berasaskan AlGaIn telah ditumbuhkan pada lapisan AlN yang optimum, iaitu pada suhu 1340 °C dan 1175 °C. LED pada lapisan AlN di suhu 1340 °C memancarkan panjang gelombang pada ~270 nm, manakala LED pada lapisan AlN di suhu 1175 °C memancarkan pada ~280 nm. Walaubagaimanapun, kedua-dua LED menunjukkan voltan hadapan yang sangat rendah disebabkan oleh kelimpahan arus yang sangat teruk.

EPITAXIAL GROWTH OF III-V NITRIDES BASED LIGHT EMITTING DIODES BY METAL ORGANIC CHEMICAL VAPOR DEPOSITION

ABSTRACT

This research aims to improve the performance of indium gallium nitride (InGaN) based LEDs and to demonstrate a working aluminum gallium nitride (AlGaN) based LEDs through metal organic chemical vapour deposition epitaxy. The effect of gallium nitride (GaN) nucleation growth temperature, superlattice period, and indium composition on InGaN based LED performance was studied. It was found that growing GaN nucleation at 570°C reduced threading dislocations (TDs) in the overgrown GaN layer (which served as the LED base layer). At 570°C nucleation, larger 3D growths (islands) formed, promoting dislocation inclination, and thus reducing TDs. Subsequently, 20 periods of $\text{In}_{0.04}\text{Ga}_{0.96}\text{N}/\text{GaN}$ SLs led to reasonable V-pits size. This increased holes injection into the multiquantum well and hence, improved the LED performance. This research also attempted to find out factors which limit the use of GaN substrates in InGaN based LEDs development over sapphire substrates, particularly pattern sapphire substrate (PSS), which is widely used in many studies, including in this research. The results revealed that the LED on PSS performed better than the one on GaN substrate, despite the latter showed lower TDs. The formation of V-pits and carrier localization, which were more obvious in the LED on PSS than the LED on GaN, led to low forward voltage and high radiative recombination, and therefore, improved the LED performance. In the subsequent stage of this research, the influence of nitridation time, AlN nucleation thickness, and trimethylaluminum (TMAI) preflow for AlGaN based LEDs were investigated. The TDs in the overgrown AlN layer grown at 1340°C (which served as the LED base

layer) were reduced through 20 minutes of nitridation. The aluminium oxynitride, which resulted from the nitridation, suppressed the TDs. The TDs were further reduced by introducing a 10 nm AlN nucleation layer. Under this condition, 3D growths favoured more dislocation inclinations in the subsequent AlN growth. This research also attempted to grow AlN layer at 1175 °C. To improve the AlN quality, the TMAI preflow time was optimized after the nucleation. With 30 seconds of TMAI preflow, the mixed polarity of Al and N was suppressed and therefore smoothed the AlN surface. Next, AlGaN based LEDs were grown on the optimized AlN layers, grown at 1340 °C and 1175 °C. The LED on 1340 °C grown AlN layer emitted at ~270 nm, while the LED on 1175 °C grown AlN layer emitted at ~280 nm. Nevertheless, both LEDs showed lower forward voltages due to severe leakage current.

CHAPTER 1

INTRODUCTION TO III-V NITRIDE SEMICONDUCTOR

Nowadays, light emitting diodes (LEDs) have been considered as an essential lighting source. This because the LEDs technology has driven efforts towards achieving sustainable energy supply and security, which in line with Sustainable Development Goals (SDGs) number 7¹ by United Nation (UN). In comparison to traditional incandescent lamp or bulbs, LEDs can convert more than 95% of input electrical energy into light. Hence, this has led to wide adoption of LEDs. Visible LEDs, especially blue LEDs, have become an essential component for white LEDs, which are used for lighting applications, screen displays and automotive headlamps. Based on latest market reports, blue LEDs are valued at USD 75.81 billion in 2020, and their value could reach up to USD 160.30 billion by 2026 [1]. On the other hand, ultraviolet (UV) LEDs have also driven motivations and excitement nowadays since the LEDs are required for advanced applications in bio-sensing, water purification, medical sterilization, and disinfection. Recently, UV LEDs are proven to eliminate coronaviruses, which cause COVID-19 disease [2]. Recent market reports for UV LED was valued at USD 0.35 billion in 2020 and could reach USD 1.71 billion by 2027 [3].

III-V nitrides (In,Ga,Al)N semiconductor materials have been widely recognized as excellent materials for developing LEDs. This is because III-V nitride materials have wider and direct bandgap, which allows optoelectronics devices based on them to operate in wide lighting spectrum, from infrared to UV. Additionally, these

¹ Goal 7: Ensure access to affordable, reliable, sustainable, and modern energy for all. SDGs are a collection of 17 interlinked global goals designed to be a "blueprint to achieve a better and more sustainable future for all".

materials exhibit outstanding thermal and chemical resilience, which then enable major breakthroughs in high temperature, high power, and high frequency applications. In Malaysia context, blue and UV LEDs have become a priority towards making the country as a known LEDs supplier in the world.

1.1 Progress and challenges of blue and UV LEDs

Blue LEDs are developed primarily using InGaN materials. Most of existing InGaN based blue LEDs in the market are about 80 % efficient [4]. Further efforts to increase the LEDs efficiency are still on-going. One of the main challenges to achieve this is to reduce Threading dislocation (TDs) in the LEDs. It is well known that high density of TDs in MQW deteriorates the LED performance. TDs are commonly generated when LEDs are grown on foreign substrates due to the difference in the lattice parameters of the materials of the LEDs and the substrates. At this point, sapphire is the most popular substrate used for blue LEDs. Such dislocations can propagate into the overgrown LEDs. When the dislocations reach multiquantum-well (MQW) active region of the LEDs, non-recombination centres are created. The centres limit the radiative recombination and thus, leads to significant degradation of the internal quantum efficiency (IQE) and the overall performance of the LEDs.

An ideal approach to minimize the TDs generation is by growing the LEDs on native substrate, e.g. bulk GaN. However, in comparison to sapphire, GaN substrates are expensive and only exist in small size of less than 2 inches. Since InGaN based LEDs are typically grown on sapphire substrate, a low temperature GaN nucleation layer has to be grown. Such layer acts as a buffer layer to reduce the impact from the lattice mismatch between GaN and sapphire. Typically, the

growth of the nucleation layer occurs at the initial stage prior to the GaN layer, which serves as the base layer for the LEDs layer. The key parameters to develop high quality GaN is by controlling GaN nucleation temperature. Therefore, manipulating the growth of the GaN nucleation prior to the GaN layer should be given more serious attention.

On the other hand, p-GaN always exhibits low hole concentration, hence, leads to poor hole injection into the MQW of the LEDs. This decreases the number of electrons and holes to recombine and subsequently produces light. Magnesium (Mg) is a common dopant for p-GaN. It is well known that the limitation of p-type GaN conductivity is due to high activation energy of Mg which ranges from 200 to 270 meV [5]. Despite of manipulating p-GaN layer growth conditions, the hole injections into the MQW of the LEDs can be enhanced by introducing V-pits through InGaN/GaN superlattices (SLs) [6]. Numerous reports have revealed that V-pits can help to lower the voltage of an LED, e.g. [7]. This is because V-pits promote thinner MQW thickness and, subsequently, can enhance the injection of holes into MQW active region. One of the key parameters to develop better injection of hole into MQWs is by controlling size and the density of V-pits. By manipulating the V-pit size and density, better hole injection to MQW is expected.

In the past few decades, considerable efforts have been made on developing aluminum gallium nitride (AlGaN) based ultra-violet (UV) LEDs since such LEDs have a huge potential for a variety of applications, primarily for disinfecting water, surfaces, and air [8-9]. A high-energy bandgap of AlGaN materials is suitable candidate for UV LEDs as they enable to emit the light emission with wavelengths of below 390 nm. In general, UV spectrum can be divided into three regions, which known as UV-A (315-360 nm), UV-B (280-315 nm) and UV-C (210 -280

nm). Among these three regions, UV-C LEDs are currently witnessing a huge demand due to their potential in fighting bacterial [8] and coronaviruses such as Middle East respiratory syndrome (MERS) [10], and most recently reported pandemic COVID-19 [11].

In comparison to blue LEDs, progress of UV LEDs is rather slow and, hence challenging. At present, progress on AlGa_N based UV-A LEDs is on-going with EQE exceeding 50%. Meanwhile, EQE for UV-B and UV-C is on average below 10% [5]. In order for UV-C LEDs to be better than mercury lamps and other traditional UV sources, their efficiency must be more than 25%. [12]. Similar to blue LEDs, one of the main challenges in the development of UV LEDs is associated to the presence of high TDs in the LEDs. As compared to blue light, UV light is prone to be absorbed by TDs [5]. Therefore, TDs in AlGa_N based LEDs could significantly decrease the efficiency, as compared to the case for InGa_N based LEDs. The use of bulk AlN substrate is the most ideal route to minimize TDs for AlN layer and hence, AlGa_N based UV LEDs. Yet, the price of the substrate is also expensive and limited in size. At present, UV LEDs are mostly grown on sapphire substrate. Such heteroepitaxial growth always suffers from high dislocations, which is in the range of 10^9 - 10^{10} cm⁻². In general, the initial stage of growth is crucial for reducing the TDs generation in the AlN layer. Therefore, more focused on the initial growth should be carried out to realize a high quality AlN template for the base layer for AlGa_N based LEDs.

1.2 Problem statement and novelty of the research

So far, InGa_N based LEDs are typically grown on sapphire substrates. Due to high lattice mismatch between Ga_N (the base layer of the LEDs) and sapphire

substrate (~16%), the LEDs always suffer from a high density of threading dislocations (TDs). The TDs can propagate into the MQW active region of the LEDs, acting as non-recombination centers which consequently deteriorate the overall LEDs performance. A high quality GaN layer for the LEDs can be obtained through epitaxial lateral overgrowth (ELOG) method. This method is able to lower the TDs generation of around 10^6 - 10^7 cm⁻² [13]. Nevertheless, this method requires for a complex lithography step during the growth interruption. Alternatively, growing a low temperature GaN nucleation layer prior to the GaN growth has been proposed as a simple method to obtain a high quality GaN layer. It is worth noting that nucleation temperature is one of the key parameters to guarantee the TDs reduction [14-15]. If the temperature is too low (e.g. below 500 °C), ammonia (NH₃) cracking would be not effective and this disturbs the GaN growth process due to the lack of nitrogen supply. If it is too high, this can result in a reduced concentration of NH₃ and therefore lower the growth efficiency of GaN. Therefore, the temperature should be precisely controlled, and this has not been well-done by far. This research attempts to investigate closer the effect of the nucleation temperature (within the range of 550 to 610 °C) on reducing the TDs in the overgrown GaN layer.

Additionally, p-GaN always exhibits a low conductivity, resulting in a poor hole injection into the MQW of the LEDs. One of the proposed approaches to improve the hole injection is by introducing V-pits through InGaN/GaN superlattices (SLs) [6]. Several studies have reported that the V-pits generation can be controlled by changing the SLs period or indium (In) composition in the SLs [16-18]. At this point, the combined effects of SLs period and In composition has never been considered. This research intends to fill-in this research gap and

anticipates that a reasonable V-pit size and density lead to a better hole injection to MQW.

Currently, commercially available InGaN based LEDs are grown on sapphire, in particular, on patterned sapphire substrate (PSS). The patterns promote light scattering that reduce total internal reflection and thereby, increasing the light extraction efficiency of the LEDs. Similar to what has been discussed above, InGaN based LEDs on sapphire exhibit TDs on the order of $10^8 - 10^{10} \text{ cm}^{-2}$ [19]. An ideal route to address this problem is to grow the LEDs on bulk GaN substrate. This is because the GaN lattice parameters nearly match to the nitrides materials which developed the LEDs. A significant reduction of the TDs in the LEDs can be as low as 10^6 cm^{-2} . Supposedly, the performance of the LEDs grown on GaN substrate should be better than that grown on PSS. Nonetheless, some published works showed that the overall efficiency of the LEDs grown on PSS is still higher than the LEDs grown on GaN substrate. The justifications of this behaviour are still unclear. This research aims to find the answer by focusing on the V-pits formation and optical carrier localization/confinement of both LEDs.

At present, ultra-violet (UV) LEDs are mostly grown on AlN/sapphire templates due to limited availability of bulk AlN substrates. Such heteroepitaxial growth, however, always suffers from high TDs in the range of $10^9 - 10^{10} \text{ cm}^{-2}$. Therefore, it is essential to achieve high quality AlN/sapphire templates with TDs of below 10^9 cm^{-2} . Up to now, several approaches have been proposed such as ELOG [20], high temperature annealing [21], and ammonia pulse-flow [22], and the TDs are reported to be on the order of 10^8 cm^{-2} . Nevertheless, the approaches demand for additional steps, which are time consuming and expensive. It is worth noting that AlN nucleation layer, of which grown at the early stage of the AlN

growth should be given a serious attention. Until now, there is less focus on controlling the AlN nucleation growth, particularly optimizing its nitridation and thickness, despite this approach can simply reduce the TDs. While the AlN nucleation temperature is found to influence the overgrown AlN layers [23-24], nitridation (pre-treatment on the sapphire surface by flowing ammonia prior to growth) and nucleation thickness are potentially improving 3D-growth islands formation, which can promote TDs inclination and hence, their mutual annihilation, leading to further TDs reduction. The scope of this work is demonstrated in this research.

1.3 Aim and objectives of research

The aim of this research is to develop improved performance of InGaN based LEDs and to demonstrate a working AlGaIn based LEDs through MOCVD epitaxy. Therefore, the main objectives of this research are;

- 1) to determine optimum nucleation temperature for reducing TDs in GaN/PSS template (GaN layer on PSS substrate) and enhancing injection carrier of holes through SLs period and indium composition to realize improved performance of InGaIn based LED.
- 2) to determine optimum nitridation, nucleation and TMAI preflow for reducing TDs in AlN/sapphire template (AlN layer on sapphire substrate) to realize a working AlGaIn based LED.

1.4 Scope of research

This research demonstrates epitaxial growth of III-V nitrides based LEDs by MOCVD. In order to improve the performance of blue LEDs, reducing of TDs in the GaN base layer is crucial. To achieve this, GaN nucleation was optimized by

controlling the growth temperature prior to GaN/sapphire template. By optimizing the nucleation temperature, a reasonable GaN islands size can be controlled properly. These islands enable to promote lateral growths, which lead to dislocation inclinations during the GaN growth and subsequently, to reduce the TDs. Further improvement of the LEDs can be enhanced by introducing V-pits formation using superlattices (SLs) layer in the LEDs structure. This was done by optimizing the number of periods of SLs and the indium (In) composition in order to obtain reasonable V-pits structure in term of size and density. With a proper control of V-pits generation, the hole injection from the p-GaN layer into the MQW could be enhanced. Subsequently, the growth of InGaN based LEDs on PSS and on GaN substrate was carried out using the optimum growth conditions from GaN nucleation layer and InGaN/GaN SLs. In general, the growth of InGaN based LEDs on bulk GaN substrate could reduce the TDs due to almost similar lattice matching. In this regards, many people believed LEDs on GaN can be the ultimate LED performance. Nevertheless, bulk GaN at the moment is still expensive and make more effort to establish this technology. At present, commercially available InGaN based LEDs are grown on sapphire substrate, particularly in patterned sapphire substrate (PSS). Despite of that, high TDs is always expected in the LEDs. Therefore, this research would like to highlight the relevant of using PSS and its potential in LED development in industry context. This is covered in this research.

In the second part of this research, reducing of TDs in AlN layer can be achieved by controlling the growth of the nitridation, which performed by flowing ammonia. This treatment will form a thin aluminum oxynitride (AlON) on the surface of the substrate, which allow the overgrown AlN layer to be grown in parallel to sapphire substrate orientation and thus, suppressed the TDs generation. Under appropriate nitridation time, reasonable AlON formation can be controlled properly

and subsequently, reduction of the TDs can be expected. Further reduction of TDs in AlN layer can be achieved by optimizing the AlN nucleation thickness. By optimizing the nucleation thickness, the size of the AlN islands can be controlled properly. This would promote more lateral growths that lead to more dislocation inclinations during the AlN growth and subsequently, reduces the TDs further. In general, high quality AlN is grown at the temperature above 1200 °C. However, only a few MOCVD are equipped with high heater setting since high temperature growth can shorten the lifetime of the heater and thus making such AlN difficult to reproduce universally. Therefore, this research took the challenge to demonstrate low-temperature grown AlN layer, which at 1175 °C. The motivation is to explore the possibility of growing AlN at a temperature below 1200 °C, which is a known common temperature for most standard MOCVD reactors. This research would pave the way for more exploration of AlN research by using a standard MOCVD reactor. Despite that, growing the AlN layer at temperature below 1200 °C can reduce the material quality due to low Al atom mobility. In order to obtain a comparable result to the AlN layer grown at high temperature, introduction of trimethylaluminum (TMAI) preflow, which is a new technique, was proposed, and applied after the nucleation layer to enhance the adatom migration. By controlling TMAI preflow time, enlargement of AlN islands and suppressing of unwanted N-polarity can be optimized and thus improve the low-temperature grown AlN layer. Subsequently, an attempt to demonstrate a working AlGaN based UV-C LEDs grown on the optimum AlN layers, grown at temperatures above 1200 °C and 1175°C was presented at the end of this research.

1.5 Outline of the thesis

This thesis is organized as follows:

Chapter 2 describes basic properties of III-V nitride materials, particularly GaN and AlN materials. Subsequently, issues for growing the materials through MOCVD epitaxy are discussed. Following that, development of InGaN and AlGaN based LEDs are reviewed.

Chapter 3 explains experimental works which had been done in this research. This also includes a description of MOCVD for atmospheric pressure and horizontal flow reactor. Furthermore, details characterization measurements to assess the surface, crystalline structure, optical and electrical properties of the grown samples are given. Moreover, steps to obtain good results are discussed. Issues, which encountered during the measurements, are explained and this followed by proposed steps to minimize the impacts of the issues.

Chapter 4 begins with works on epitaxial growth of InGaN based LEDs by atmospheric pressure MOCVD reactor. In particular, by optimizing growth conditions of GaN nucleation to obtain good GaN layer grown on PSS and by controlling number of SLs period and In composition. This is followed by comparing the characteristics of the InGaN based LEDs grown on PSS and on GaN substrate. Next, this chapter discusses research on epitaxial growth of AlGaN based LEDs by horizontal flow MOCVD reactor. In particular, by controlling the duration of nitridation and the thickness of AlN nucleation layer grown on sapphire with the growth temperature at 1340 °C. This is subsequently followed by optimizing the duration of TMAI preflow, which was applied after the nucleation layer to obtain good AlN layer grown on sapphire with the growth temperature at 1175 °C. Towards the end, optimized AlN layers are used to demonstrate working AlGaN based LEDs.

Chapter 5 summarizes findings of this work. This is followed by suggestions for future works for extending the scope of this research.

CHAPTER 2

LITERATURE REVIEW

This chapter begins with an overview of III-V nitride materials and its basic properties and followed by preferable growth technique for III-V nitrides LEDs. This includes theoretical background for basic LEDs concept will be given. Next, review on issues and challenges related to developing the materials from the aspect of growth are discussed. This is followed by the works that have been done on advancing III-V nitrides LEDs growth.

2.1 Introduction to III-V nitride materials

III-V nitride materials or (AlGaIn)N are semiconductor compounds which compose of elements from group III i.e., gallium (Ga), aluminum (Al) and indium (In), and group V, that is nitrogen (N). Theoretically, it is well known that III-V nitrides materials allow LEDs and laser diodes based on them to operate in a wide spectrum range from near infrared to ultraviolet. Despite of that, producing red LEDs are challenging. This is because red LEDs require high indium content in InGaN based LEDs. In general, high indium content exhibits newly dislocation generation due to large difference in lattice constants with respect to GaN which produce highly strain layer. Furthermore, high indium content also exhibited Ga- In phase separation, which make it difficult to achieve red LEDs [25]. By far, current red LEDs available in market are based on aluminum indium gallium phosphide (AlInGaP) instead of InGaN based materials. Figure 2.1 shows lattice constant in *a*-direction of AlGaInN materials with their corresponding bandgap energy and wavelength. As seen in figure 2.1, III-V nitrides cover a wider range of bandgap energy which is advantages for producing a

wide range of optoelectronic devices. In fact, today, III-V nitrides are the mainstream materials in development of LEDs with applications such as for screen displays, horticulture, automotive headlamps, medical disinfection devices and laser diodes, as well as other electronic devices such as high electron mobility transistor (HEMT), photodetector and solar cell [26].

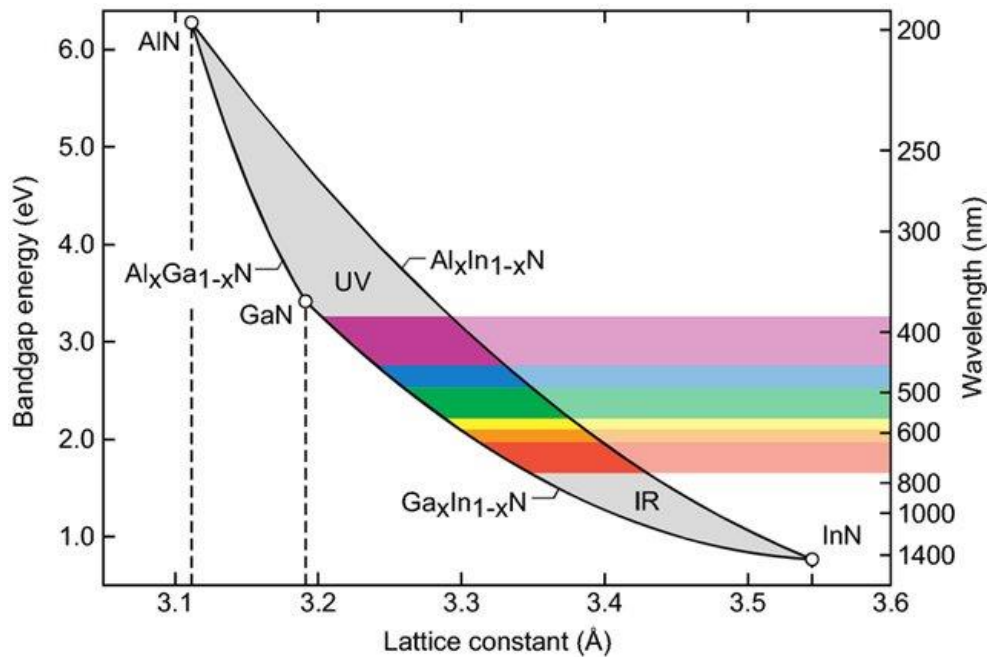


Figure 2.1: Energy bandgap of III-V nitrides in the function of lattice constant a at room temperature. Image taken from [26].

In general, III-V nitride materials are formed in thermodynamically stable wurtzite (hexagonal) crystal structure. It consists of two lattice constants, which is a and c . Lattice constant, a refers to the distance between two atoms at a basal plane. Meanwhile, c is associated to the distance, which is perpendicular to the basal plane. The atomic arrangement for hexagonal III-V nitride is shown in figure 2.2. Each atom from group III (Al, Ga, In) is bonded to four neighboring N atoms. Likewise, each N atom is also bonded to four group III atoms (see figure 2.2). The stacking sequence for the hexagonal III-nitrides in the $\langle 0001 \rangle$ plane is ABABAB along the c -axis, where

the capital A is referred to distinctive of (Al, Ga, In) cation whilst the capital B is denoted as N anion position in the triangular lattice on the (0001).

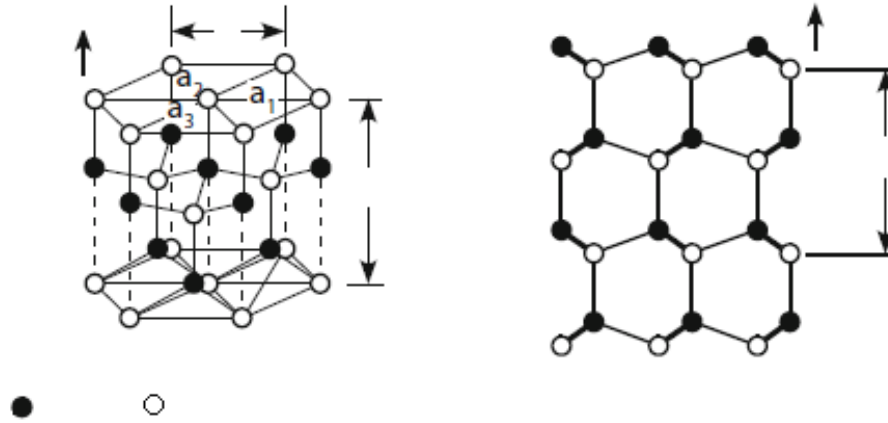


Figure 2.2: Atomic arrangement for wurtzite structure of nitride materials. The images were taken from [27].

Table 2.1 shows the properties of hexagonal GaN, AlN and InN, at 300 K. The values shown in the table are typically reported in many works, for example in [28-29]. It should be noted that these values vary with different growth conditions. Theoretically, the arrangement of atoms depends on the strain-induced defects inside the grown materials. This subsequently influences the crystalline properties of the materials. In general, the composition of group-III in nitride materials changes the properties of the materials. For example, the energy bandgap of the materials [29]. Ternary alloy, e.g. $\text{In}_x\text{Ga}_{1-x}\text{N}$ for visible and $\text{Al}_x\text{Ga}_{1-x}\text{N}$, for UV LEDs, are commonly grown to develop quantum wells of the LEDs, where the light emission is generated. Hence, the emission wavelength of the LEDs depends on the composition of the materials of the quantum wells. For example, 18 %-20 % of In in InGaN is required to achieve an emission at 450 nm [30-32], 25-30% of In in InGaN for 550 nm [33-35] and 15- 18 % of Al in AlGaN for 280 nm [5]. However, introduction of ternary alloys

will result in highly strained heterostructures owing to large mismatch in lattice constants among the binary nitrides. This can lead to defect formation, reduced material quality and polarization-related electric fields in the overgrown layer.

Table 2.1: Common parameters of binary III-nitride materials at 300 K. The values were taken from [28-29,36-38].

Structure	InN	GaN	AlN
Symmetry	Hexagonal	Hexagonal	Hexagonal
Structure	Wurtzite	Wurtzite	Wurtzite
Stability	Stable	Stable	Stable
Energy Gap (eV)	0.70	3.42	6.20
Nature of Energy Gap	Direct	Direct	Direct
Energy Gap (eV) at 300K	0.70	3.42	6.20
Wavelength (nm)	1771.43	362.57	200.00
Lattice constant, a (Å)	3.548	3.186	3.111
Lattice constant, c (Å)	5.760	5.185	4.978
Density at 300K	6.81 g/cm ³	6.1 g/cm ³	3.255 g/cm ³
Molar mass	128.83 g/mol	83.730 g/mol	40.989 g/mol
Melting point	1,100 °C	>1600°C	2,500 °C
Electron mobility at 300 K	3200 cm ² /Vs	1500 cm ² /Vs	~300 cm ² /Vs
Thermal conductivity at 300 K	45 W/(m.K)	1.3 W/(cm·K)	2 W/(cm·K)
Thermal diffusivity	0.2 cm ² s ⁻¹	0.43 cm ² s ⁻¹	1.47 cm ² s ⁻¹
Linear Thermal Expansion Coefficient at 300 K	Along a : 3.80 $\times 10^{-6}$ K ⁻¹ Along c : 2.90 $\times 10^{-6}$ K ⁻¹	Along a : 5.59 $\times 10^{-6}$ K ⁻¹ Along c : 3.17 $\times 10^{-6}$ K ⁻¹	Along a : 4.15 $\times 10^{-6}$ K ⁻¹ Along c : 5.27 $\times 10^{-6}$ K ⁻¹
Calculated Spontaneous Polarisation	-0.032 C m ⁻²	-0.029 C m ⁻²	-0.081 C m ⁻²
Calculated Piezo-electric Coefficients	e_{13} : -0.45 C m ⁻² e_{33} : +0.81 C m ⁻²	e_{13} : -0.37 C m ⁻² e_{33} : +0.67 C m ⁻²	e_{13} : -0.62 C m ⁻² e_{33} : + 1.46 C m ⁻²
Dielectric constants	$\epsilon_0 = 15.3$	$\epsilon_0 = 10$	$\epsilon_0 = 8.5$
Refractive index	2.80-3.05	2.429	2.15

High quality III-V nitrides can be obtained via molecular-beam epitaxy (MBE) [39-40], hydride vapour phase epitaxy (HVPE) [41-42] and metal-organic chemical vapour deposition (MOCVD) [6-7] or sometimes termed as metal-organic vapor phase epitaxy (MOVPE). MBE offers a relatively low growth rate, which is beneficial for quantum wells [43], quantum dots and quantum wires [44]. However, MBE is not suitable for mass production of LED since its low growth rate. Apart from being expensive, MBE needs ultra-high vacuum in its growth chamber.

In contrast, HVPE growth with relatively high growth rate up to 100 mm/hr is suitable for bulk layers, For example, bulk GaN and bulk AlN substrate [45]. Despite of its high growth rate, HVPE is not able to grow thin layers and is difficult to achieve abrupt surface. Meanwhile, MOCVD offers good abruptness of interface, precise control of growth rate and does not require ultrahigh vacuum. In fact, MOCVD growths are typically conducted in atmospheric pressure at 1 standard atmosphere (atm). Therefore, MOCVD is preferable for III-V nitrides LEDs and widely used in for research and for industry.

2.2 Basic concept of LED and its terminology

Light emitting diodes or typically known as LEDs are semiconductor light source that combine a p-type semiconductor (larger hole concentration) with an n-type semiconductor (larger electron concentration). When applying a sufficient forward voltage, holes from the p-type and electrons from the n-type recombine at the depletion region, releasing energy in the form of light photons. In the typical nitride LED structure, the p-type semiconductor consists of magnesium, Mg source which acts as a p-dopant, while n-type semiconductor consists of silicon, Si source which acts as a n-dopant. The depletion region can be referred to the active region zone that consists

of multiquantum wells (MQWs), e.g. InGaN/GaN MQWs, and this is where the recombination takes place. Figure 2.3 shows the principle of LEDs mechanism.

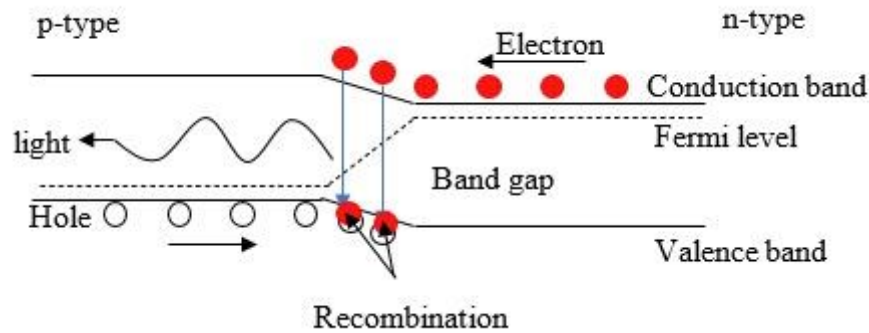


Figure 2.3: Basic working principle of an LED [26].

2.2.1. Radiative and non-radiative recombination

In general, the electron-hole recombination mechanisms can be classified into two groups: radiative and non-radiative recombination. Radiative recombination is mainly associated with band-to-band recombination and occurs when electrons in the conduction band recombine with holes in the valence band and thus emitting energy in the form of photons. In general, direct band-to-band recombination is only possible in the materials with low defect density since the defects in the crystal structure will have the possibility to trap or capture the emission from radiative recombination, thus making the recombination less favorable. This is known as non-radiative recombination [26].

Basically, non-radiative recombination can be categorized as either Shockley-Read-Hall (SRH) or Auger recombination [26,46]. SRH or trap-assisted recombination occurs when a carrier is captured at an energy level close to the conduction or valence bands, respectively. The trapped carrier will not be able to recombine with the opposite charge carrier, which results in electron-hole pair annihilation. In addition, it also results in a lower energy difference between the

conduction or valence band and the energy states of the trapped carrier. The energy is exchanged in the form of lattice vibrations known as phonons, which then exchange thermal energy with the materials, resulting in heating. This heating occurs within the material at the defect sites and can be extremely detrimental to device efficiency.

Meanwhile, Auger is the process where the excess energy from electron-hole recombination is transferred to electron or holes, which subsequently excited to higher energy states within the similar band rather than emitting photons [46]. Auger recombination becomes significant at very high injection currents or high excitation intensities and thus reduces the luminescence efficiency.

2.2.2 Quantum confinement stark effect in nitride LEDs

Because InGaN/GaN MQWs have significant strain due to the large lattice mismatch between InN and GaN, large piezoelectric polarization can exist in InGaN/GaN MQWs. The polarization-induced electric fields in InGaN/GaN MQWs result in spatial separation of the electron-hole wavefunctions, which reduces radiative recombination rates, especially for wider QW > 3 nm. This effect is known as the Quantum Confined Stark Effect (QCSE) [47]. In other words, electric fields exhibit a tilting of the energy bands that produce an accumulation of electrons close to QW interface while accumulation of holes at the opposite QW interface. Figure 2.4 illustrates the formation of QCSE in nitride LEDs. The QCSE becomes worse with increasing strain associated with increasing indium composition for longer wavelengths. Thus, high indium content, longer wavelength emitters in c-plane QW

devices have shown lower efficiencies than violet-emitting (low indium content) devices [47].

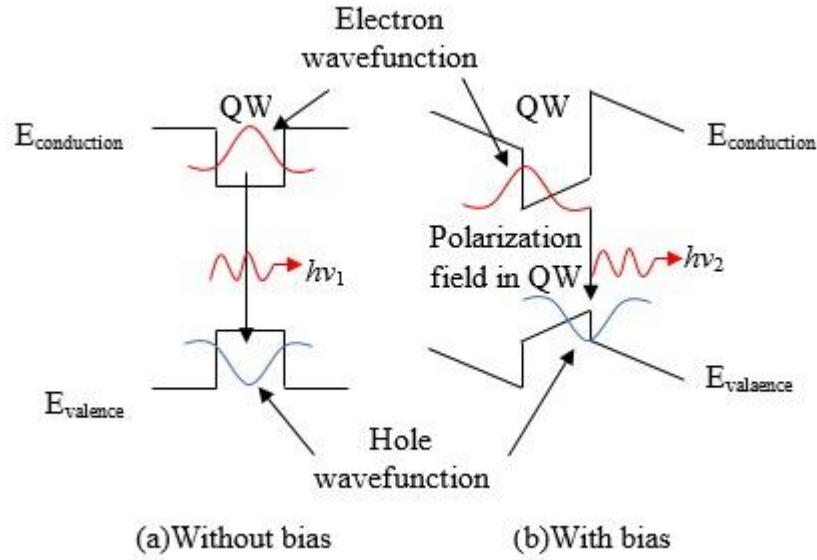


Figure 2.4: Formation of QCSE in nitride LEDs. Image taken and edited from [47].

2.2.3 Definitions of LED efficiencies

The development of high efficiency LEDs for solid state lighting requires a quantitative determination of device parameters to further improve the performance. The first common metric of an LED device is known as internal quantum efficiency (IQE). In general, an ideal case of active region of an LED emits one photon for every electron injected. However, not all electron-hole recombinations are radiative. Such an LED has unity of quantum efficiency. The IQE can be described as the fraction of electrons injected into the LED that generate photons in the active region. It can be defined as:

$$\eta_{IQE} = \frac{\text{number of photons emitted from active region per second}}{\text{number of electrons injected into LED per second}} = \frac{P_{int}/(h\nu)}{I/e} \quad (2.1)$$

where P_{int} is the optical power emitted from the active region while I is the injection current [26].

IQE is mainly connected to the quality of the active layer, which is determined by the growth conditions of the layer, such as growth pressure, temperature, quality and flow of gases and precursors, incorporation of impurities, as well as growth technique, the type of reactor used, and by the choice of substrate. These conditions affect the crystalline quality, defect density of the grown material, uniformity, doping profile and also surface morphology.

The second common metric of LED device is known as light extraction efficiency (LEE). In ideal case, all photons emitted by the active region should escape from the LED chip into free space. Nevertheless, in real LED emitter, not all the power emitted from the active region is emitted into free space due to several possible loss mechanisms, such reabsorption from the substrate of the LED, blockage from the metallic contact surface and also due to total internal reflection [26]. Therefore, the light extraction efficiency can be described as the fraction of photons generated in the active region that are emitted to free space. It can be defined as:

$$\eta_{\text{extraction}} = \frac{\text{number of photons emitted into free space per second}}{\text{number of photon emitted from active region per second}} = \frac{P/(hv)}{P_{\text{int}}/hv} \quad (2.2)$$

where P is the optical power emitted into free space. LEE is primarily determined by LED architecture e.g the use of patterned substrate [48], surface roughening [49-50], chip design [51], some dependence with material absorption and reflection. Therefore, LEE can be a hindrance to achieving high-performance LEDs.

The third common metric of LED is known as external quantum efficiency (EQE). EQE refers to the fraction of electrons injected into the LED, which generate

photons that are emitted into free space [52]. EQE can also be expressed as the product of IQE and LEE as:

$$\text{EQE} = \text{IQE} \times \text{LEE} \quad (2.3)$$

To optimize EQE, it requires structures with low contact resistance and high conductivity materials, including efficient heat sink to maintain high performance under all operating conditions [53]. In addition, the EQE gives the fraction of the input power (IV) that is converted to optical output power, known as wall-plug efficiency (WPE) [26]. WPE is related to EQE by the voltage drop, V at the device due to the forward voltage and series resistance and can be expressed by

$$\eta_{\text{WPE}} = \frac{P_{\text{out}}}{VI} \quad (2.4)$$

where I is the injected current.

In general, WPE and EQE can be easily measured from the applied current in the integrating sphere [54]. Meanwhile, IQE and LEE are not easily measured. The IQE is widely estimated by temperature-dependent photoluminescence (PL) while the LEE is commonly estimated by using simulations and models, e.g ray tracing methods to approximate their values [46,55].

2.2.4 Carrier screening and band-filling effect in InGaN based LEDs.

One of the methods to measure the LED spectrum is by using electroluminescence (EL). The peak wavelength of the emitted light can be measured with increasing injected current, and one can monitor the shift in wavelength known as the “blue-shift” phenomenon. This blue-shift phenomenon was attributed to two possible reasons such as the carrier screening effect and the band filling effect [56-57]. Both effects play different roles in the observed EL characteristic and can be

analyzed by the peak wavelength and full width at half maximum (FWHM) at different injection currents.

In general, carrier screening effect can be interpreted by the screening of the huge strain-induced piezoelectric field in the nitride materials. If the strain is smaller in the nitride materials, the piezoelectric field is weaker, and a smaller density of the injected carriers could fully screen its effect [56]. The blueshift of the emission peak will stop when the piezoelectric field is close to being fully screened. Meanwhile, the blueshift and broadening of the FWHM of the emission wavelength with higher injection current is known as band filling [57]. At higher current densities, radiative recombination from higher energy states will occur since there are more injected carriers and the possibility of injected carriers being filled at higher energy states is greater. Figure 2.5 shows the schematic of band diagram for the carrier screening effect and the band filling effect.

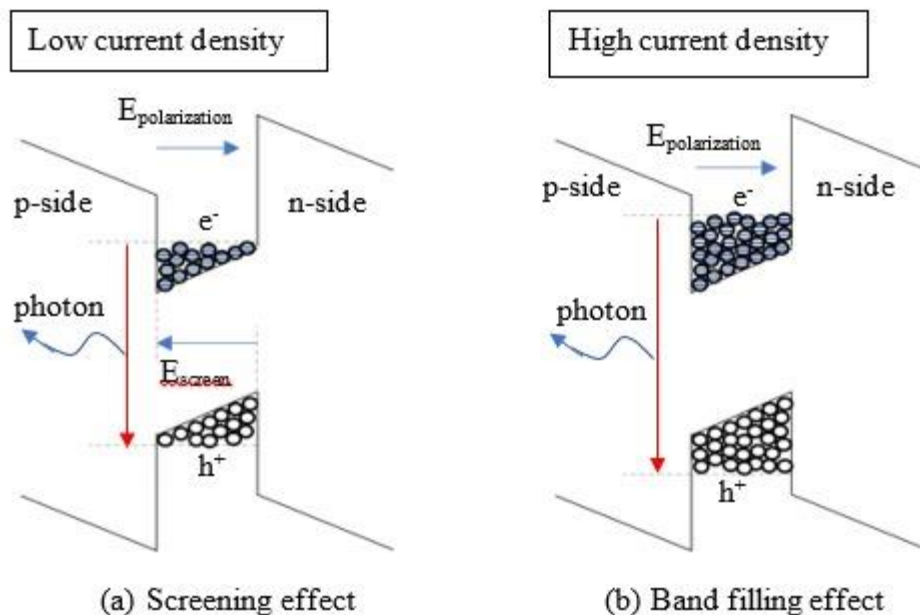


Figure 2.5. The schematic diagram for (a) screening effect and (b) band filling effect in the InGaN based LEDs. Image taken and edited from [57].

2.2.5 Carrier localization in InGaN based LEDs.

Despite high dislocation densities in nitride based III-V devices, there are many works reported that their efficiency is still high, e.g. [58]. The most accepted explanation for this behavior is that carriers are localized before they have a chance to reach dislocation density. There are three possible reasons for this carrier localization that have been widely cited, random alloy fluctuations [59], well width fluctuations [60], and indium clustering [61].

Random InGaN alloy fluctuation possibly happens due to large difference in bandgap between GaN and InN, which could create fluctuations in potential energy that enough to localize the carriers [59]. In the case of well width fluctuations, there is a large change in confinement energy for only a monolayer change in well width due to the strong piezoelectric field within InGaN/GaN structures. In combination with the roughness of the top interface layer, this could be enough to localize the carriers and explain this highly efficient luminescence [60]. The most popular theory that could cause the carrier localization is that carriers are thought to localize at indium rich sites within the active region. Indium was thought to develop clusters as the InGaN was being grown and was supported theoretically and experimentally, for example in [61].

Photoluminescence (PL) is commonly used to observe the evidence of carrier localization. It involves illuminating an InGaN/GaN LED sample with laser light energy above the band gap. This excitation produces electron-hole pairs within the bulk GaN, which then diffuse into the active region where they recombine by emitting photons, scanning the intensities across a range of energies, then building up a spectrum. PL spectrum can provide useful information regarding the lowest lying energy states in the system, which are at the bottom of quantum well. The relative

intensity peak of PL provides information regarding the quality of the sample, the width of the peak indicates structural or compositional inhomogeneity, and the peak position can provide the quantum well shape.

In addition, the relative intensity of the PL peak can also change with temperature, where the intensity reducing with temperature. This ‘quenching’ can be clarified by the thermalization of the carriers out of confining potential with an activation energy related to the depth of the confining potential. This confining energy can be estimated by fitting the curve using an Arrhenius plot (a plot of relative intensity versus inverse temperature). Figure 2.6 illustrates the thermal quenching of the carriers out of confining potential.

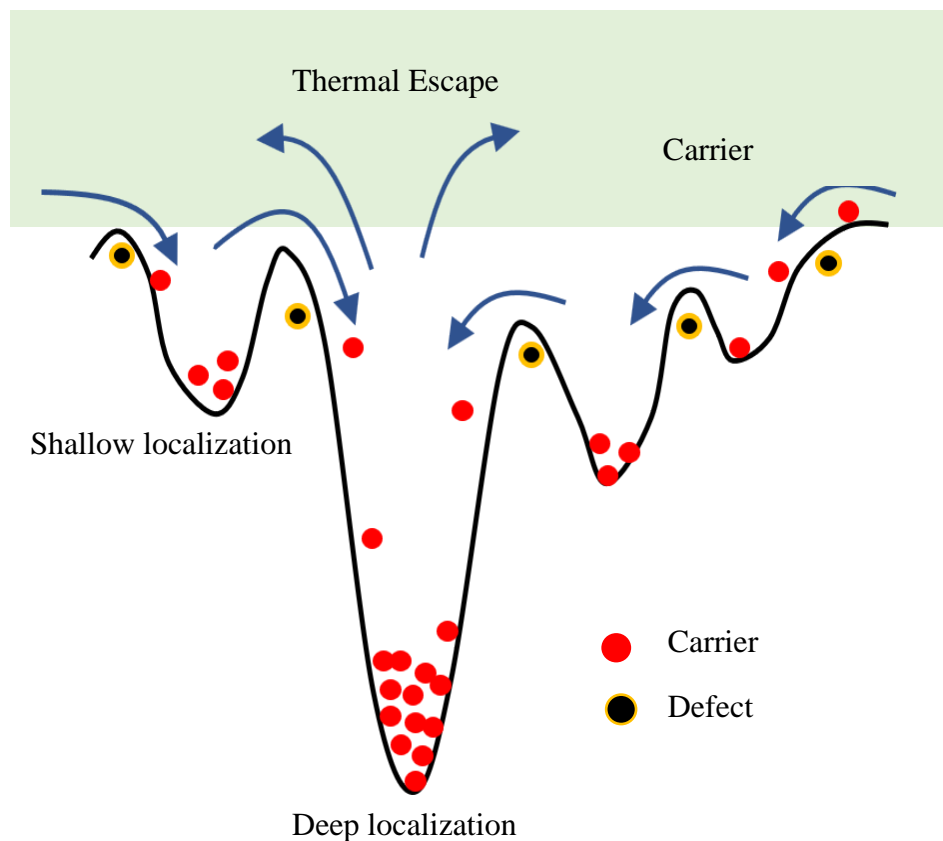


Figure 2.6. Illustration of thermal quenching in QW. Image taken and edited from [61].